Occurrence of the collective Ziman limit of heat transport in cubic semiconductors Si, Ge, AlAs and AlP: scattering channels and size effects

Jelena Sjakste, Maxime Markov, Raja Sen, Giorgia Fugallo, Lorenzo Paulatto, Nathalie Vast

PAPER

Occurrence of the collective Ziman limit of heat transport in cubic semiconductors Si, Ge, AlAs and AlP: scattering channels and size effects

Jelena Sjakste[1], Maxime Markov[1], Raja Sen[2], Giorgia Fugallo[3], Lorenzo Paulatto[2] and Nathalie Vast[1]

[1] Laboratoire des Solides Irradiés, CEA/DRF/IRAMIS, Ecole Polytechnique, CNRS, Institut Polytechnique de Paris, F91128 Palaiseau cédex, France

[2] Sorbonne Université, Museum National d'Histoire Naturelle, UMR CNRS 7590, Institut de Minéralogie, de Physique des Matériaux et de Cosmochimie, 4 place Jussieu, F-75005 Paris, France

[3] Laboratoire de Thermique et Energie de Nantes, CNRS, UMR 6607, Université de Nantes, Nantes, 44306, France

E-mail: jelena.sjakste@polytechnique.edu

Keywords: heat transport, lattice thermal conductivity, hydrodynamic regime, second sound, semiconductors, density functional theory

Abstract

In this work, we discuss the possibility of reaching the Ziman conditions for collective heat transport in cubic bulk semiconductors, such as Si, Ge, AlAs and AlP. In natural and enriched silicon and germanium, the collective heat transport limit is impossible to reach due to strong isotopic scattering. However, we show that in hyper-enriched silicon and germanium, as well as in materials with one single stable isotope like AlAs and AlP, at low temperatures, normal scattering plays an important role, making the observation of the collective heat transport possible. We further discuss the effects of sample sizes, and analyse our results for cubic materials by comparing them to bulk bismuth, in which second sound has been detected at cryogenic temperatures. We find that collective heat transport in cubic semiconductors studied in this work is expected to occur at temperatures between 10 and 20 K.

1. Introduction

The study of the heat transport regimes in bulk and low dimensional materials in general, and of the phonon hydrodynamics in particular, currently attracts a renewed interest [1–13], both from theoretical and experimental viewpoints. The discussion of recent advances can be found in the review article of [4].

In most of the literature until very recently, a regime in which phonons behave not as independent carriers but as a collective excitation [14, 15] which manifests itself in the form of the second sound temperature wave or of the Poiseuille flow, is referred to as the hydrodynamic regime. Indeed, the hydrodynamic behaviour is expected to occur in the limit where momentum-conserving 'normal' phonon-phonon scattering processes dominate over resistive scattering processes. However, it was pointed out recently [2, 3] that this collective Ziman limit is not the only regime in which non-Fourier effects can be observed [3, 6]. As wave-like heat transport at the nanoscale [3, 6] is also referred to as hydrodynamic heat transport in literature [6], and to avoid confusion, in this work we follow the clarification of [2] and discuss the collective (or Ziman) limit of heat transport, rather than the hydrodynamic regime.

The heat flow regimes in suspended graphene and graphene nanoribbons were studied very actively [8, 16–22] since the prediction, by *ab initio* methods, of the occurrence of a collective transport regime in graphene nanoribbons [18–21]. Recently the Poiseuille flow of phonons was experimentally observed in black phosphorus [9], graphite [1, 7, 23, 24] and $SrTiO_3$ [25]. All of these materials have particular distinct features in their phonon dispersion facilitating 'normal' momentum-conserving scattering processes necessary to reach the collective limit. The first two materials, as well as graphene, belong to the group of 2D- or layered systems in which the non-linear out-of-plane flexural phonon mode plays the role of the efficient scattering channel which accumulates decaying phonons from linear acoustic branches. $SrTiO_3$ is an 'incipient ferroelectric' with a 'falling' optical polar phonon mode at the Brillouin zone center which strongly decreases in frequency when the

temperature is decreased but, in contrast to real ferroelectrics, is eventually stabilized by quantum fluctuations [26, 27]. Moreover, recently coherent second sound waves were observed in a dense magnon gas [28]. At the same time, the collective limit of heat transport was observed only in relatively few 'common' 3D materials, such as Bi [29, 30], solid helium [31], and NaF [32, 33] at cryogenic temperatures. In materials such as natural Si and Ge, the dominance of resistive processes, and in particular scattering by isotopes, prevents the occurrence of the collective limit. Indeed, the damping of the peak of thermal conductivity at low temperatures was demonstrated in many works, as one of the main effects of the isotopic disorder [34, 35] on the material properties, with respect to isotopically enriched materials [1, 36–41]. At the same time, we note that in contrast to the collective limit, the 'high-frequency', or 'driftless' second sound was recently observed in bulk Si and Ge [3, 6] in a rapidly varying temperature field. As it was pointed out in [3], in the latter case the dominance of the normal scattering events is not necessary to observe wave-like heat transport, the slow decay of the energy flux being the key requirement instead.

Turning back to the collective limit of heat transport, methods based on the density functional perturbation theory and on the Boltzmann transport equation (BTE) were shown to accurately predict the conditions of the occurrence of the collective limit in many materials [4, 5, 21, 23, 42]. It is expected to occur in samples with sizes defined by the interplay between normal phonon scattering (τ_N), phonon-boundary (τ_b) and resistive scattering (τ_R) times [42], under the condition: $\tau_N < \tau_b < \tau_R$. Note that while the above-described approach can be used to provide the indication that the conditions for the occurrence of the collective transport are present (or absent), as we aim to do in this work, it is not suitable to describe the collective heat transport phenomena. Instead, the collective heat transport can be described with approaches based on the macroscopic hydrodynamic equation [6, 43, 44] or the mesoscopic kinetic equation [2, 45].

In the present work, we apply the approach similar to the one of [42] or [5] to discuss the conditions of the occurrence of the collective limit of heat transport in cubic semiconductors, such as silicon, germanium, AlAs and AlP, as a function of isotope composition and at temperatures below 50 K. Experimentally, thermal conductivity of enriched and hyper-enriched Si were studied e.g. in [40, 41], whereas enriched and hyper-enriched Ge was studied experimentally in [37], between 4 K and 300 K. We show that in materials with one single stable isotope, such as AlAs and AlP, or in isotopically hyper-enriched silicon, the collective limit of heat transport can be reached at temperatures between 10 and 20 K, where the normal scattering dominates. We show that the reason for the absence of the collective limit in natural silicon and germanium is the isotopic scattering, and that collective heat transport phenomena such as 'drifting' second sound could in principle be observed in hyper-enriched silicon and germanium samples, which become available nowadays [46].

2. Methodology and computational details

2.1. Methodology

To identify the conditions for the occurrence of the collective limit of phonon transport, we use the solution of the BTE beyond the single-mode approximation (SMA), which allows to explicitly take into account the repopulation of phonon states. The lattice thermal conductivity obtained in the SMA approximation is denoted κ_{SMA}, whereas the lattice thermal conductivity obtained with the variational approach to BTE is denoted κ_{VAR}.

We use the ratio $\kappa_{VAR}/\kappa_{SMA}$ as the criterion of the occurrence of the collective regime. Momentum-conserving phonon-phonon scattering processes repopulate the heat-carrying phonon states, leading to the difference between the SMA and full solution of BTE. Note that other scattering processes, such as specular border scattering, which was not considered in this work, may also lead to important repopulations of phonon states. We also compare the thermodynamic average scattering rate of 'normal' (momentum conserving) phonon-phonon scattering processes, Γ^n_{av} to resistive Umklapp phonon-phonon scattering rate, Γ^U_{av}, as well as to other resistive scattering rates due to isotopic scattering, and to boundary scattering [42]. The thermodynamic averages of different phonon-scattering rates are calculated as [42]: $\Gamma_{av} = \frac{\sum_\nu C_\nu \Gamma_\nu}{\sum_\nu C_\nu}$, where C_ν is the specific heat of the phonon mode ν. We note that in this work, we consider isotropic cubic crystals, in which all transport directions are equivalent, and thus there is no need to consider direction-dependent averages of scattering rates, as it has to be done in highly anisotropic materials [7].

2.2. Computational details

Si, AlAs, and AlP are described within the density functional theory in the local density approximation with norm-conserving pseudopotentials [47]. Harmonic force constants were computed on a $8 \times 8 \times 8$ **q**-point sampling of the Brillouin zone (BZ) using the Density Functional Perturbation theory (DFPT) [48] as implemented in the QUANTUM ESPRESSO package [49]. Third-order anharmonic constants of the normal and Umklapp phonon interactions have been computed on a $4 \times 4 \times 4$ **q**-point grid in the BZ using the DFPT formalism as implemented in the D3Q package [50] and then Fourier-interpolated on the denser $30 \times 30 \times 30$ grid necessary for converged integrations of the phonon-phonon scattering rates [50, 51]. The lattice thermal conductivity has been computed with the linearized Boltzmann transport equation and the variational method

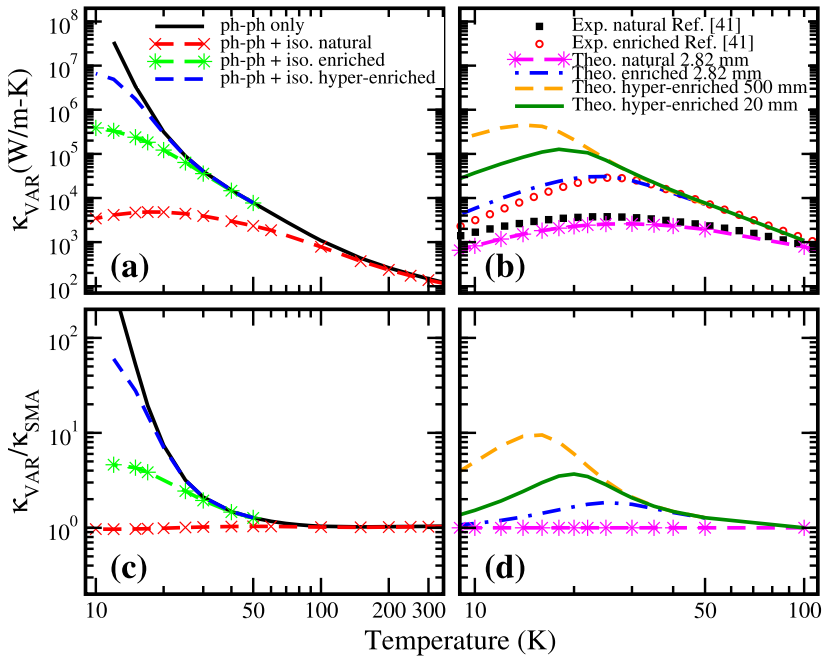

Figure 1. Panels a and c: the lattice thermal conductivity κ_{VAR} and the ratio $\kappa_{VAR}/\kappa_{SMA}$ for Si without boundaries. Black solid line—pure silicon with phonon-phonon scattering mechanism only; Red, blue and green dashed-dotted lines—natural, enriched and hyper-enriched silicon with phonon-phonon + isotopic scattering. Panels b and d: the lattice thermal conductivity and the ratio $\kappa_{VAR}/\kappa_{SMA}$ for Si with boundaries, for different millimetric sample sizes.

on a $30 \times 30 \times 30$ **q**-point grid with the smearing parameter $\sigma = 2\ \mathrm{cm}^{-1}$ [51, 52]. Phonon-boundary scattering is modeled by the Casimir model with the cylindrical geometry for millimeter-sized wires [51, 53, 54], in the completely diffusive limit with no specularity [42, 55]. Isotope scattering in Si is described with the widely used Tamura model [51, 53, 56, 57] with the scattering probability:

$$P^{iso}_{j\mathbf{q},j'\mathbf{q}'} = \frac{\pi}{2N_0}\omega_{j\mathbf{q}}\omega_{j'\mathbf{q}'}\left[n_{j\mathbf{q}}n_{j'\mathbf{q}'} + \frac{n_{j\mathbf{q}} + n_{j'\mathbf{q}'}}{2}\right] \times \delta(\hbar\omega_{\mathbf{q}j} - \hbar\omega_{\mathbf{q}'j'})\sum_s g_s \left|\sum_\alpha z^{s\alpha}_{\mathbf{q}j} z^{s\alpha}_{\mathbf{q}'j'}\right|^2 \quad (1)$$

where s run over all atoms, α is the Cartesian coordinate index, j is the phonon branch index, $\mathbf{q}$ is the phonon wavevector, $z^{s\alpha}_{\mathbf{q}j}$ is the phonon eigenmode, $\omega_{\mathbf{q}j}$ is the phonon frequency, $g_s = \frac{(M_s - \langle M_s\rangle)^2}{\langle M_s\rangle}$ is the mass variance parameter. As Al, As and P are monoisotopic elements, with only one single stable isotope, AlAs and AlP are naturally isotopically pure materials, which were not studied as a function of isotope composition.

All computational parameters were subjected to usual convergence tests. The figure illustrating the convergence of the low-temperature lattice thermal conductivity with respect to the Brillouin zone sampling, calculated within the SMA and the variational BTE approach is provided in the appendix.

3. Results: calculated thermal conductivity

3.1. Phonon state repopulation in Si and isotope scattering effect

In panel a of figure 1, we show the thermal conductivity (without boundary) calculated within the variational approach to BTE for natural silicon, isotopically enriched silicon, and extra-pure silicon which became available recently [46], and which we will refer to as 'hyper-enriched Si' in the present work. The isotopic compositions of Si studied in our work are summarized in table 1. In panel b, we show our results for the thermal conductivity of silicon in presence of boundary scattering. In presence of boundary scattering, our calculated thermal conductivity of Si with various isotopic compositions is found in good agreement with available experimental data [40, 41]. We note that our calculations of the lattice thermal conductivity of Si, as well as those of AlAs and AlP which will be discussed later, are also in agreement with previous *ab initio* calculations [58, 59] (previous theoretical data of [59] has been obtained for the 100-400 K temperature range).

In panel c of figure 1, we show the ratio $\kappa_{VAR}/\kappa_{SMA}$, for Si with various isotopic compositions. At room temperatures and down to 70 K, the ratio $\kappa_{VAR}/\kappa_{SMA}$ is equal to one for all samples, which is a clear signature of

Table 1. Silicon. Composition, average mass M_{av} (in atomic mass units) and the isotopic disorder parameter g_s for hyper-enriched ([46]), enriched, and natural silicon.

	Composition	M_{av}	g_s
hyper-enriched	Si^{28}-99.9995%, Si^{29}-0.0005%	27.98	$6.38 \cdot 10^{-9}$
enriched	Si^{28}-99.983%, Si^{29}-0.014%, Si^{30}-0.003%	27.98	$3.31 \cdot 10^{-7}$
natural	Si^{28}-92.23%, Si^{29}-4.67%, Si^{30}-3.10%	28.09	$2.01 \cdot 10^{-4}$

the kinetic regime, where heat is transported by single phonon modes. However, as one can see in panel c, the ratio $\kappa_{VAR}/\kappa_{SMA}$ for isotopically pure silicon attains two orders of magnitude below 20 K (black curve), and similar results are obtained for hyper-enriched silicon (blue dashed curve), demonstrating the importance of the normal processes and of the repopulation for pure and hyper-enriched samples below 20 K. Therefore, the possibility of the collective heat transport limit is not excluded for these samples. In contrast, one can see that the collective heat transport limit is not possible in natural silicon according to our analysis (red dashed curve with crosses), and in agreement with common knowledge. Indeed, the $\kappa_{VAR}/\kappa_{SMA}$ ratio is close to one, and thus one can conclude that the resistive processes dominate and that the repopulation does not play any important role in the latter case. In the isotopically enriched silicon case (green dashed curve with stars), the $\kappa_{VAR}/\kappa_{SMA}$ ratio is much larger than that of the natural silicon, however, there is no temperature regime in which it attains one order of magnitude.

According to our results, the same conclusions are valid for germanium (results not shown): in natural and isotopically enriched samples, the possibility of the collective heat transport limit which could potentially exist in hyper-enriched or pure samples, is destroyed by isotopic scattering.

In order to further investigate the possibility of the collective heat transport limit in the isotopically hyper-enriched silicon and to compare with experiments, we include boundary scattering. In panels b and d of figure 1, we show the thermal conductivity of Si and the ratio $\kappa_{VAR}/\kappa_{SMA}$ for various isotopic compositions and in presence of boundary scattering for different sample sizes. In panel b, our computational results for 2.82 mm sample size, for natural and enriched silicon, are compared with the experimental results of [40, 41]. As one can see, the agreement between calculated and experimental thermal conductivity is very good. To illustrate the effect of sample size on the lattice thermal conductivity, we also show the calculated results in hyper-enriched silicon for the 20 mm and 500 mm sizes.

As one can see in panel d of figure 1, as expected, the ratio $\kappa_{VAR}/\kappa_{SMA}$ is reduced in presence of the boundary scattering, for all sizes and all isotopic compositions. Nevertheless, normal processes play an important role for hyper-enriched samples, especially for sample sizes of 20 mm and above.

The possibility of the collective heat transport limit in isotopically enriched samples of 2.82 mm size was discussed in [40]. As one can see in panel d of figure 1, we find indeed that the ratio $\kappa_{VAR}/\kappa_{SMA}$ for those samples (blue dot-dashed curve) exceeds 1 for temperatures between 10 K and 60 K, with the maximum value of 1.8 at 25 K, confirming the conclusions of [40] that the collective heat transport can exist to some extent. However, the effect of the repopulation of phonon states by the normal processes is strongly reduced by the isotopic and boundary scattering for 2.82 mm samples.

3.2. Repopulation in AlAs and AlP

In the previous section, we have demonstrated that the isotopic scattering is the main reason why the collective limit can not be observed in Si and Ge, while it could exist in pure or hyper-enriched samples. This is the reason why we have decided to further explore cubic materials that naturally have no isotopes, such as AlP and AlAs.

In upper panel of figure 2, we show our calculated lattice thermal conductivity for AlP and AlAs, as a function of temperature. In lower panel of figure 2, in analogy with the analysis of figure 1, we show the ratio $\kappa_{VAR}/\kappa_{SMA}$ for AlP and AlAs. One can see that, similarly to pure Si, the $\kappa_{VAR}/\kappa_{SMA}$ ratio for AlP attains two orders of magnitude around 17 K. The same is true for AlAs, at slightly lower temperatures around 8 K. Thus, we conclude that according to our results, repopulation due to normal processes is very strong in AlP and AlAs at low temperatures. Therefore, the collective transport limit can also exist in AlP and AlAs. Also, we can conclude that contrary to common belief, normal processes play an important role in cubic materials such as Si, AlP and AlAs, but at temperatures below 20 K, and when isotopic scattering is absent or strongly reduced. In the next section, we further analyse the effect of sample sizes.

4. Discussion: size effects and scattering rates

The effect of boundary scattering, analysed in panel d of figure 1 for silicon, appears to be very strong. Indeed, the $\kappa_{VAR}/\kappa_{SMA}$ between 10 and 20 K for hyper-enriched samples is reduced by almost two orders of magnitude, from about one hundred (panel c, blue dashed curve) to 3.7 in 20 mm samples (panel d, green curve).

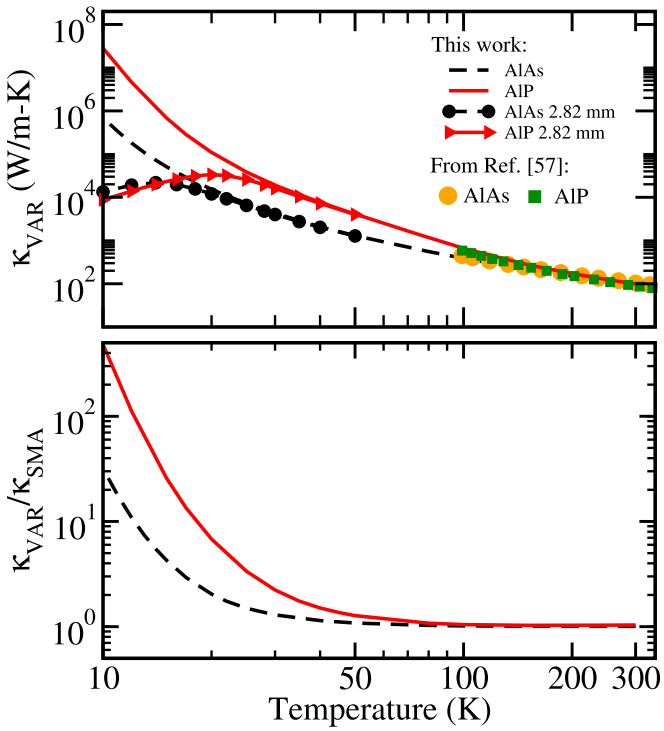

Figure 2. Upper and lower panels : the lattice thermal conductivity κ_{VAR} and the ratio $\kappa_{VAR}/\kappa_{SMA}$ for AlP and AlAs. Red solid and black dashed lines—AlP and AlAs respectively with phonon-phonon interaction only. Lines with symbols: results for samples with 2.82 mm boundaries.

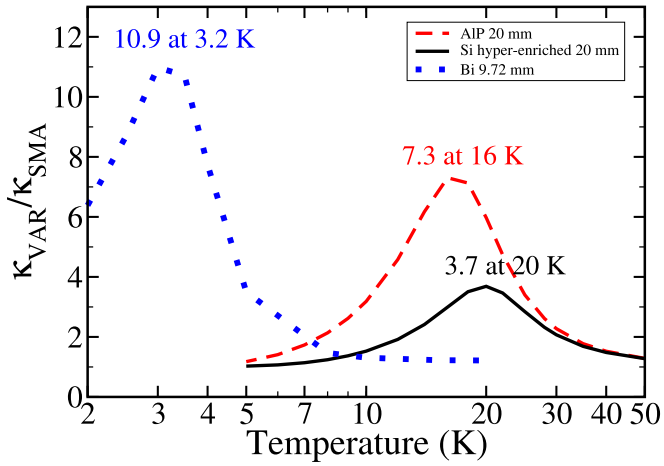

Figure 3. $\kappa_{VAR}/\kappa_{SMA}$ ratio for AlP and hyper-enriched Si samples of 20 mm, compared to $\kappa_{VAR}/\kappa_{SMA}$ ratio for Bi sample of 9.72 mm.

In figure 3, we compare $\kappa_{VAR}/\kappa_{SMA}$ ratios in hyper-enriched silicon, cubic AlP and bismuth, which was studied in our earlier works [42, 54]. The interest in comparing materials studied in the present work with Bi resides in the fact that the collective heat transport (drifting second sound) was experimentally observed in the latter [29]. As one can see in figure 3, scattering by boundaries reduces the repopulation effects in all three materials. We can also note that the effect of repopulation reduction by boundary scattering appears to be somewhat weaker in Bi, resulting is larger peak value of $\kappa_{VAR}/\kappa_{SMA}$ ratio. At the same time, the peak value of $\kappa_{VAR}/\kappa_{SMA}$ in AlP at 16 K for 20 mm sample is still comparable to that of Bi at 3.2 K for 9.72 mm sample, indicating that observation of the collective heat transport limit in AlP must be possible at temperatures around 16 K for 20 mm samples.

To further understand why the effect of repopulation reduction by boundary scattering is stronger in Si and AlP compared to Bi, we study the average scattering rates in figure 4. By comparing the Umklapp and normal

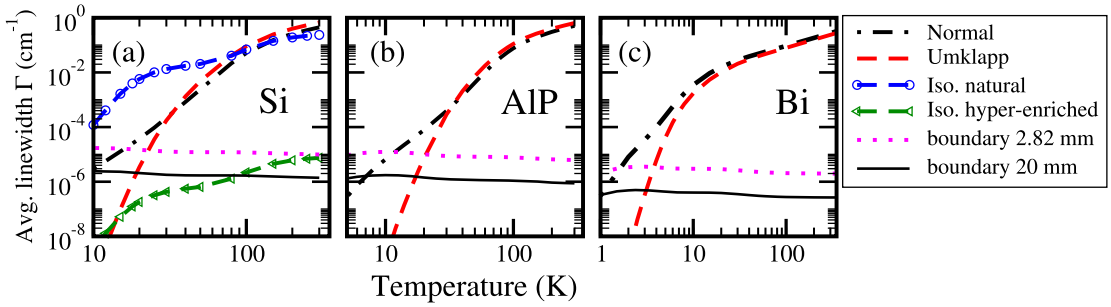

Figure 4. The thermodynamic average of phonon linewidth. Black dot-dashed lines — normal processes, red dashed lines — Umklapp processes; blue and green lines with symbols — isotopic scattering for natural and hyper-enriched silicon. Horizontal lines: boundary scattering for 2.82 mm (red dotted line) and 20 mm (black solid line) samples.

scattering rates in panels a (Si), b (AlP) and c (Bi) of figure 4, we notice that overall, in all three materials the normal scattering dominates over the Umklapp scattering at low temperatures. In that respect, cubic materials studied in this work are similar to Bi. The major role of isotopic scattering, which is the dominant scattering process below 70 K in natural silicon, is also illustrated in panel a of figure 4.

Coming now to boundary scattering rates, we notice that for equal sample sizes, boundary scattering rates are 4 to 5 times larger in Si and AlP, compared to Bi. This fact, which is due to larger phonon group velocities in Si and AlP as compared to those in Bi, explains why the repopulation reduction by boundary scattering is stronger in Si and AlP.

5. Conclusions

In this work we have performed the theoretical analysis of the conditions necessary to reach the collective heat transport limit in silicon with various isotopic compositions, as well as in AlAs and AlP which contain naturally one single stable isotope. While the collective heat transport is impossible in natural silicon due to isotopic scattering, it can in principle be reached in hyper-enriched Si, as well as in natural AlAs and AlP. We have shown that, contrarily to common belief, the normal phonon-phonon scattering processes can play an important role in the examined cubic semiconductors below 20 K, similarly to Bi where collective heat transport phenomena have been experimentally observed. In addition, in the cubic materials studied in this work, the possibility to reach the collective heat transport limit is reduced by the large phonon group velocities that enhance the effect of boundary scattering with respect to, e.g. bismuth. Nevertheless, as we have shown in the present work, the observation of the collective heat transport limit in AlP must be possible at temperatures around 16 K for 20 mm samples.

Acknowledgments

Calculations have been performed with the Quantum ESPRESSO computational package [49] and the D3Q code [50, 51]. We are grateful to A. V. Inyushkin for providing the experimental data published in [40, 41]. We acknowlege useful discussions with B. Fauquet and F. Mauri. This work has been granted access to HPC resources by the French HPC centers GENCI-IDRIS, GENCI-CINES and GENCI-TGCC (Project 2210) and by the Ecole Polytechnique through the *Three Lab Computing* cluster. Financial support from the ANR PLACHO project ANR-21-CE50-0008 is gratefully acknowleged.

Data availability statement

All data that support the findings of this study are included within the article (and any supplementary files).

Appendix

In figure A1, we show an example of convergence test with respect to the **q**-point grid for the thermal conductivity calculated with the SMA and variational approach to BTE, for the case of pure silicon (no border,

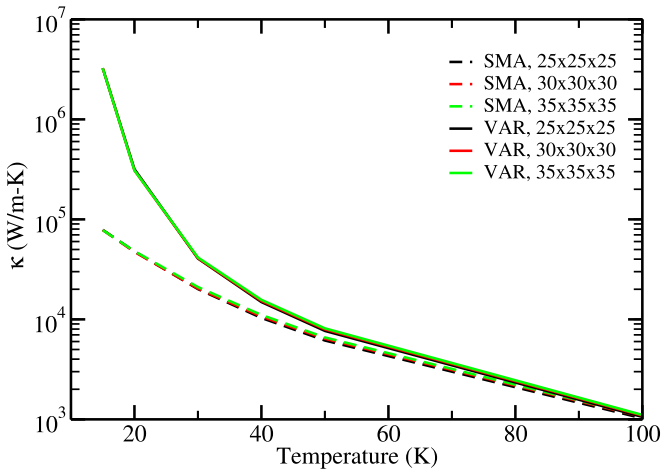

Figure A1. Convergence of the κ_{VAR} and κ_{SMA} with respect to the **q**-point grid: example of silicon with no border and no isotopes.

no isotopes). As one can see in figure A1, the calculations with 30 × 30 × 30 **q**-point grid are well converged for the temperatures discussed in this work, for both the SMA and variational approaches to BTE.

ORCID iDs

Jelena Sjakste https://orcid.org/0000-0002-3164-7400
Raja Sen https://orcid.org/0000-0002-9838-975X
Giorgia Fugallo https://orcid.org/0000-0002-1514-5726

References

[1] Ding Z, Chen K, Song B, Shin J, Maznev A, Nelson K and Chen G 2022 Observation of second sound in graphite over 200 K *Nat. Comm.* **13** 285
[2] Sendra L, Beardo A, Bafaluy J, Torres P, Alvarez F X and Camacho J 2022 Hydrodynamic heat transport in dielectric crystals in the collective limit and the drifting/driftless velocity conundrum *Phys. Rev.* B **106** 155301
[3] Beardo A *et al* 2021 Observation of second sound in a rapidly varying temperature field in Ge *Sci. Adv.* **7** eabg4677
[4] Ghosh K, Kusiak A and Battaglia J-L 2022 Phonon hydrodynamics in crystalline materials *J. Phys.: Condens. Matter.* **34** 323001
[5] Ghosh K, Kusiak A and Battaglia J-L 2021 Effect of characteristic size on the collective phonon transport in crystalline GeTe *Phys. Rev. Materials* **5** 073605
[6] Beardo A, Calvo-Schwarzwalder M, Camacho J, Myers T G, Torres P, Sendra L, Alvarez F X and Bafaluy J 2019 Hydrodynamic heat transport in compact and holey silicon thin films *Phys. Rev. App.* **11** 034003
[7] Ding Z, Zhou J, Song B, Chiloyan V, Li M, Liu T-H and Chen G 2018 Phonon hydrodynamic heat conduction and Knudsen minimum in graphite *Nano Lett.* **18** 638
[8] Machida1 Y, Matsumoto N, Isono T and Behnia K 2020 Phonon hydrodynamics and ultrahigh-room-temperature thermal conductivity in thin graphite *Science* **367** 309
[9] Machida Y, Subedi A, Akiba K, Miyake A, Tokunaga M, Akahama Y, Izawa K and Behnia K 2018 Observation of Poiseuille flow of phonons in black phosphorus *Science Advances* **4** eaat3374
[10] Cahill D G *et al* 2015 Nanoscale thermal transport. II. 2003-2012 *Applied Physics Reviews* **1** 011305
[11] Volz S *et al* 2016 Nanophononics: state of the art and perspectives *Eur. Phys. J.* B **89** 15
[12] Chang C W, Cohen Okawa D, Garcia H, Majumdar A and Zettl A 2008 Breakdown of Fourier's law in nanotube thermal conductors *Phys. Rev. Lett.* **101** 075903
[13] Yand N, Zhang G and Li B 2010 Violation of Fourier's law and anomalous heat diffusion in silicon nanowires *Nano Today* **5** 85
[14] Cepellotti A and Marzari N 2016 Thermal transport in crystals as a kinetic theory of relaxons *Phys. Rev.* X **6** 041013
[15] Cepellotti A and Marzari N 2017 Transport waves as crystal excitations *Phys. Rev. Mat.* **1** 045406
[16] Li X and Lee S 2019 Crossover of ballistic, hydrodynamic, and diffusive phonon transport in suspended graphene *Phys. Rev.* B **99** 085202
[17] Majee A K and Aksamija Z 2018 Dynamical thermal conductivity of suspended graphene ribbons in the hydrodynamic regime *Phys. Rev.* B **98** 024303
[18] Zhang J, Huang X, Yue Y, Wang J and Wang X 2011 Dynamical response of graphene to thermal impulse *Phys. Rev.* B **84** 235416
[19] Fugallo G, Cepellotti A, Paulatto L, Lazzeri M, Marzari N and Mauri F 2014 Thermal conductivity of graphene and graphite: collective excitations and mean free paths *Nano Lett.* **14** 6109
[20] Lee S, Broido D, Esfarjani K and Chen G 2015 Hydrodynamic phonon transport in suspended graphene *Nat. Commun.* **6** 6290
[21] Cepellotti A, Fugallo G, Paulatto L, Lazzeri M, Mauri F and Marzari N 2015 Phonon hydrodynamics in two-dimensional materials *Nat. Commun.* **6** 6400
[22] Luo X-P, Guo Y-Y and Yi H-L 2024 Nonlocal phonon thermal transport in graphene in hydrodynamic regime *J. Phys.: Condens. Matter.* **36** 115705

[23] Huang X, Guo Y, Wu Y, Masubuchi S, Watanabe K, Taniguchi T, Zhang Z, Volz S, Machida T and Nomura M 2023 Observation of phonon Poiseuille ?ow in isotopically purified *Nat. Comm.* **14** 2044
[24] Huberman S, Duncan R A, Chen K, Song B, Chiloyan V, Ding Z, Maznev A A, Chen G and Nelson K A 2019 Observation of second sound in graphite at temperatures above 100 K *Science* **364** 375
[25] Martelli V, Jimenez J L, Continentino M, Baggio-Saitovitch E and Behnia K 2018 Thermal transport and phonon hydrodynamics in strontium titanate *Phys. Rev. Lett.* **120** 125901
[26] Rabe K M, Ahn C H and Triscone J-M 2007 *Physics of Ferroelectrics. A Modern Perspective* (Springer)
[27] Gurevich V L and Tagantsev A K 1988 Second sound in ferroelectrics *Sov. Phys. JETP* **67** 206–12
[28] Tiberkevich V, Borisenko I V, Nowik-Boltyk P, Demidov V E, Rinkevich A B, Demokritov S O and Slavin A N 2019 Excitation of coherent second sound waves in a dense magnon gas *Sci. Rep.* **9** 9063
[29] Narayanamurti V and Dynes R C 1972 Observation of second sound in bismuth *Phys. Rev. Lett.* **28** 1461
[30] Mezhov-Deglin L P, Kopylov V N and Medvedev E S 1974 Contributions of various phonon relaxation mechanisms to the thermal resistance of the crystal lattice of bismuth at temperatures below 2 K *Sov. Phys. JETP* **40** 557
[31] Ackerman C C, Bertman B, Fairbank H A and Guyer R A 1966 Second sound in solid helium *Phys. Rev. Lett.* **16** 789
[32] Jackson H E, Walker C T and McNelly T F 1970 Second sound in NaF *Phys. Rev. Lett.* **25** 26
[33] Pohl D W and Irniger V 1976 Observation of second sound in NaF by means of light scattering *Phys. Rev. Lett.* **36** 480
[34] Haller E E 2005 Isotopically controlled semiconductors *Solid State Comm.* **133** 693
[35] Cardona M and Thewalt M L W 2005 Isotope effects on the optical spectra of semiconductors *Rev. Mod. Phys.* **77** 1173
[36] Thacher P D 1967 Effect of boundaries and isotopes on thermal conductivity of LiF *Phys. Rev.* **156** 975
[37] Ozhogin V I, Inyushkin A V, Taldenkov A N, Tikhomirov A V and Popov G E 1996 Isotope effect in the thermal conductivity of germanium single crystals *JETP Lett.* **63** 490
[38] Zhernov A P and Inyushkin A V 2002 Kinetic coefficients in isotopically disordered crystals *Phys. Usp.* **45** 527–55
[39] Lindsay L 2016 First principles peierls-boltzmann phonon thermal transport: a topical review *Nanoscale Microscale Thermophys. Eng.* **20** 67
[40] Inyushkin A V, Taldenkov A N, Gibin A M, Gusev A V and Pohl H-J 2004 On the isotope effect in thermal conductivity of silicon *Phys. Status Solidi* C **1** 2995
[41] Inyushkin A V, Abrosimov N V, Taldenkov A N, Ager J W, Haller E E, Riemann H, Pohl H-J and Becker P 2018 Ultrahigh thermal conductivity of isotopically enriched silicon *J. Appl. Phys.* **123** 095112
[42] Markov M, Sjakste J, Barbarino G, Fugallo G, Paulatto L, Lazzeri M, Mauri F and Vast N 2018 Hydrodynamic heat transport regime in bismuth : a theoretical viewpoint *Phys. Rev. Lett.* **120** 075901
[43] Guo Y and Wang M 2018 Phonon hydrodynamics for nanoscale heat transport at ordinary temperatures *Phys. Rev.* B **97** 035421
[44] Simoncelli M, Marzari N and Cepellotti A 2020 Generalization of Fourier's law into viscous heat equations *Phys. Rev.* X **10** 011019
[45] Sýkora M, Pavelka M, Restuccia L and Jou D 2023 Multiscale heat transport with inertia and thermal vortices *Phys. Scr.* **98** 105234
[46] Abrosimov N V *et al* 2017 A new generation of 99.999 enriched 28 Si single crystals for the determination of Avogadro's constant *Metrologia* **54** 599
[47] Fuchs M and Scheffler M 1999 Ab initio pseudopotentials for electronic structure calculations of poly-atomic systems using density-functional theory *Computer Physics Communications* **119** 67
[48] Baroni S, de Gironcoli S, Dal Corso A and Giannozzi P 2001 Phonons and related crystal properties from density-functional perturbation theory *Rev. Mod. Phys.* **73** 515
[49] Giannozzi P *et al* 2017 Advanced capabilities for materials modelling with QUANTUM ESPRESSO *J. Phys.: Condens. Matter.* **29** 465901
[50] Paulatto L, Mauri F and Lazzeri M 2013 Anharmonic properties from a generalized third-order ab initio approach: theory and applications to graphite and graphene *Phys. Rev.* B **87** 214303
[51] Fugallo G, Lazzeri M, Paulatto L and Mauri F 2013 Ab initio variational approach for evaluating lattice thermal conductivity *Phys. Rev.* B **88** 045430
[52] Omini M and Sparavigna A 1995 An iterative approach to the phonon Boltzmann equation in the theory of thermal conductivity *Physica* B **212** 101
[53] Sparavigna A 2002 Influence of isotope scattering on the thermal conductivity of diamond *Phys. Rev.* B **65** 064305
[54] Markov M, Sjakste J, Fugallo G, Paulatto L, Lazzeri M, Mauri F and Vast N 2016 Nanoscale mechanisms for the reduction of heat transport in bismuth *Phys. Rev.* B **93** 064301
[55] Sen R, Vast N and Sjakste J 2023 Role of dimensionality and size in controlling the drag Seebeck coefficient of doped silicon nanostructures: A fundamental understanding *Phys. Rev.* B **108** L060301
[56] Tamura S 1983 Isotope scattering of dispersive phonons in Ge *Phys. Re.* B **27** 858
[57] Omini M and Sparavigna A 1997 Heat transport in dielectric solids with diamond structure *Il Nuovo Cimento* D **19** 1537
[58] Ward A, Broido D A, Stewart D A and Deinzer G 2009 Ab initio theory of the lattice thermal conductivity in diamond *Phys. Rev.* B **80** 125203
[59] Lindsay L, Broido D A and Reinecke T L 2013 Ab initio thermal transport in compound semiconductors *Phys. Rev.* B **87** 165201